Ab Initio Study of the Reaction Mechanism of CH_3^+ and CH_3^- with CH_2═CNa(OH)

Yi-gui Wang,*,†,‡ Michael Dolg,† Wen-sheng Bian,‡ and Cong-hao Deng‡

Max-Planck Institute of Physics of Complex Systems, Nöthnitzer Street 38, D-01187 Dresden, Germany, and Institute of Theoretical Chemistry, Shandong University, Jinan, Shandong 250100, People's Republic of China

Received: September 18, 1998; In Final Form: December 28, 1998

The reactions $CH_3^+ + CH_2$═$CNa(OH) \rightarrow CH_2$═$C(CH_3)(OH) + Na^+$ and $CH_3^- + CH_2$═$CNa(OH) \rightarrow CH_2$═$C(CH_3)Na + OH^-$ have been investigated at the RHF/6-31+G* ab initio level of theory. The electron correlation contributions were evaluated at the MP2(fu)/6-31+G* level of theory at the RHF/6-31+G* optimized structures. The first reaction needs CH_2═CNa(OH) to change from three-member-ring **1** to nonplanar structure **4**, and the carbenoid mechanism does not work. The second reaction has a planar transition state similar to the metal-stabilized carbenium **2**, and this transition state indicates that the "metal-assisted ionization" mechanism is likely to happen.

Introduction

In the search of efficient acylation reagents in organic synthesis, α,*β*-unsaturated α-alkali metal ethers were found to be very useful. They are not only easily prepared and they can react under moderate conditions, but also their workup is easy.[1−4] In view of the synthetic method, they belong to the so-called "Umpolung" reagents, which are able to invert their polarity of the reactive center. On one hand, they readily react with electrophiles. On the other hand, such reagents can also react with nucleophiles R′Li to replace their OR group by R′, which is the typical reaction only of carbenoids.[5−7] The two different characters motivated us to investigate the geometry of the model molecule CH_2═CNa(OH) and to predict possible reaction mechanisms using the frontier molecular orbital (FMO) approach.[8] However, it is well-known that the prediction of reaction mechanisms only at the basis of FMO may have potential defects. Thus, we decided to study the prototype reactions CH_2═CNa(OH) + $CH_3^+ \rightarrow CH_2$═$C(CH_3)(OH) + Na^+$ and CH_2═CNa(OH) + $CH_3^- \rightarrow CH_2$═$CNa(CH_3) + OH^-$ in this paper.

Computational Method

Analytical gradient methods[9] based on the restricted Hartree−Fock (RHF) wave function obtained with 6-31+G* basis sets[10] were used throughout to investigate the geometries of CH_2═CNa(OH), the reaction intermediates, and products, as well as the transition states. Because the systems investigated here have a large number of electrons, the RHF level of theory was employed in all geometric optimizations. The contributions of electron correlation to the energy profile were evaluated in single-point calculations by employing second-order Mφller−Plesset perturbation theory (MP2) at the MP2(fu)/6-31+G* level of theory. Frequencies were calculated at the RHF/6-31+G* level of theory to confirm the equilibrium structures and transition states and to evaluate the zero-point vibration energies (ZPE, scaled by 0.8929[11]). To know how the charge distribution changes, the natural population analysis (NPA) method[12] was used. For troublesome transition states such as **5**, **10**, and **19**, the intrinsic reaction coordinates (IRC) method[13,14] was used to follow the reaction paths. For transition states **16** and **19**, solvent effects were calculated with the self-consistent reaction field (SCRF) method,[15,16] and further calculations at higher levels of theory than MP2(fu)/6-31+G*//RHF/6-31+G* are also given. All calculations were carried out with the Gaussian 92[17] and Gaussian 98[18] program packages on a Silicon Graphics workstation.

Result and Discussion

I. Geometry and Isomerization of CH_2═C(OH)Na. The optimized geometries of the possible equilibrium structures of CH_2═CNa(OH) and the corresponding transition states are depicted in Figure 1. The corresponding RHF/6-31+G* total energies, ZPEs (scaled by 0.8929), MP2(fu)/6-31+G* single point energies, and relative energies are given in Table 1, in which the previously published MP2/6-31+G*//MP2/6-31+G* results[8] are also given for comparison.

Like the results at the MP2/6-31+G* level of theory, the RHF/6-31+G* calculations reveal that CH_2═CNa(OH) has four possible equilibrium structures(**1**−**4**). Structure **1** contains a Na coordinated to the α-C and O is the most stable structure. The classical structure **3** is about 20−30 kJ/mol and structure **4**, with Na only bonded to O, is 30−40 kJ/mol higher in energy. Structure **2**, the metal-stabilized carbenium, is by far the richest in energy among the four structures.

We have two alternative ways to explain the stabilities of the different structures. The first model considers a carbanion (see figure below, left). When the hydrogen on C_2 of vinyl alcohol is removed, the resulting anion can be stabilized by the Na^+ cation in two ways: (1) Coulomb attraction between the carbanion and the metal cation or formation of a C−Na bond. (2) Interaction of the lone pair of oxygen with Na^+.

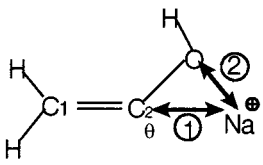

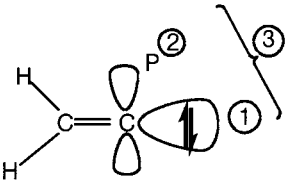

† Max-Planck Institute of Physics of Complex Systems.
‡ Shandong University.

10.1021/jp983782f CCC: $18.00
Published on Web 04/16/1999

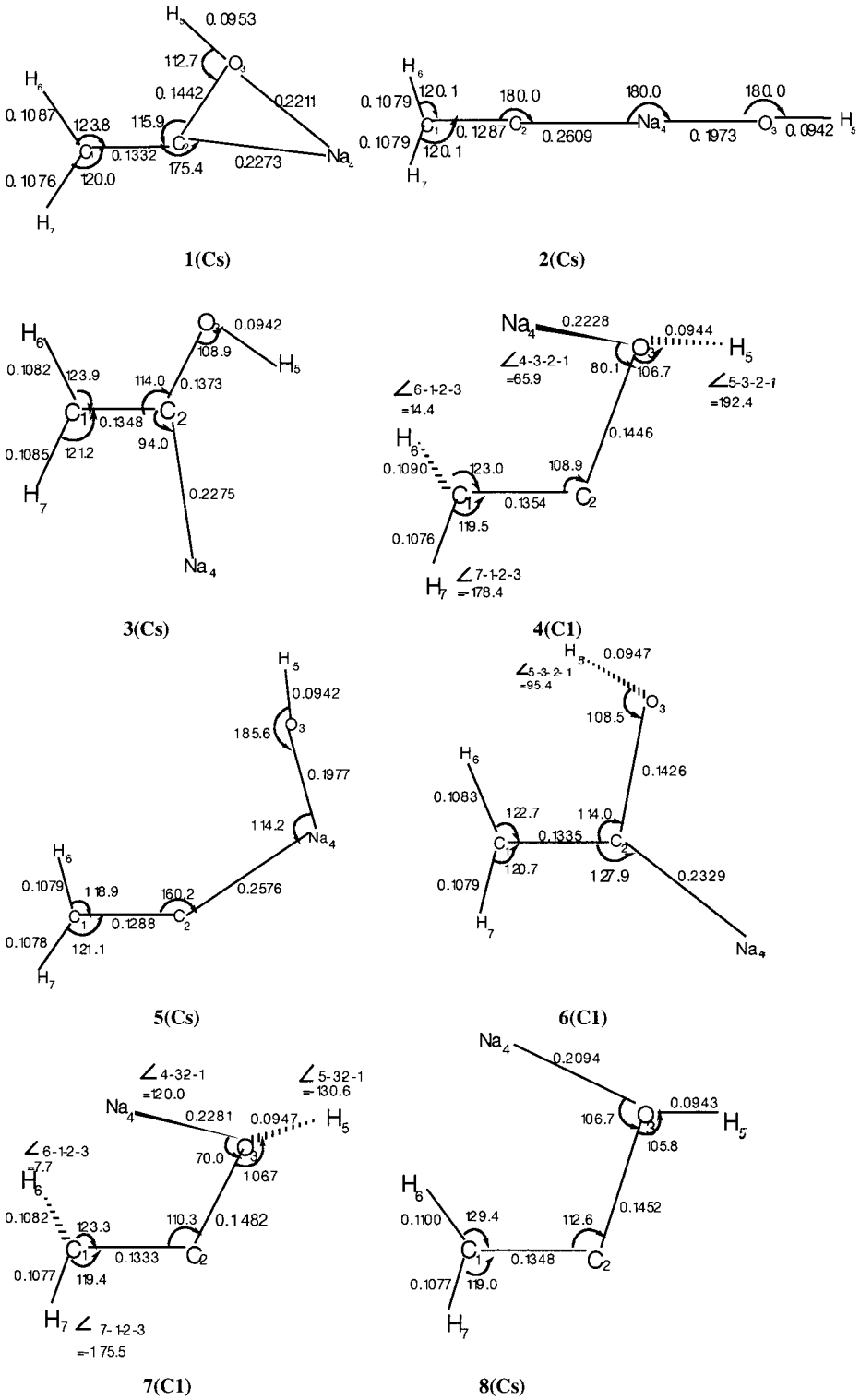

Figure 1. Local minima and transition states for CH_2=C(OH)Na (RHF/6-31+G*, bond lengths in nm, bond angles in deg).

Structure **1** possesses both stabilizing factors and is the most stable structure. Structure **4** is stabilized only by the second factor, while structure **3** only by the first one. Because the C_2-anion of vinyl alcohol already has a weak C_2−O bond due to the unfavorable "Umpolung" of C_2 carbon, the Na^+ cation further helps to break the C_2−O bond leading to structure **2**.

The second way starts from a carbene (see figure above, right). The ground state of methylidenecarbene (CH_2=C:) is a singlet, in which one carbon orbital is empty and the second contains two spin-paired electrons. Here NaOH can undergo three interactions: (1) Only the positive Na tail of NaOH interacts with the C_2 electron pair, which gives structure **2**. (2) Only a lone pair of the negative O part interacts with the p-empty orbital on C_2, which gives structure **4**. (3) Both Na and O interact with the C_2 electron pair and the empty p-orbital, respectively, which gives the most stable structure **1**. The slightly less stable structure **3** is obtained from structure **1** by cleavage of the Na−O bond.

Structures **5**−**8** are the four corresponding transition states. Structure **1** can change into **2**, **3**, and **4** through the transition states **5**, **6**, and **7**, respectively. Structure **8** is the transition state between **4** and its mirror-image. Two facts confirm the conclu-

TABLE 1: Total Energies, *E* (au), ZPE[a] (kJ/mol), and Relative Energies, Δ(*E* + ZPE) (kJ/mol), for CH_2=C(OH)Na

	RHF/6-31+G*			MP2(fu)/6-31+G*//6-31+G*		MP2/6-31+G*//MP2/6-31+G* [8]	
structure	*E*	ZPE	Δ(*E* + ZPE)	*E*	Δ(*E* + ZPE)	*E*	Δ(*E* + ZPE)
1	−314.125 18	123.6	0.0	−314.594 83	0.0	−314.532 79	0.0
2	−314.077 43	104.6	108.4	−314.529 96	153.3	−314.474 63	152.7
3	−314.117 49	124.4	20.9	−314.583 14	31.4	−314.524 22	22.5
4	−314.113 26	124.2	31.8	−314.580 11	39.1	−314.521 26	30.3
5	−314.076 19	105.2	112.1	−314.527 33	160.7	−314.473 28	156.2
6	−314.108 05	121.6	43.1	−314.575 17	49.8	−314.517 33	40.6
7	−314.111 04	123.3	36.9	−314.579 93	38.8	−314.520 73	31.7
8	−314.098 55	121.7	68.2	−314.564 60	77.7	−314.504 66	73.9

[a] ZPEs are calculated at the RHF/6-31+G* level of theory and scaled by a factor 0.8929.

sions: (1) A frequency analysis shows that all transition states have a single imaginary frequency and otherwise regular vibrational mode. The reaction vectors for the transition states **5**−**8** are separately as follows (only the dominant parts are given): **e**(**5**) = 0.11804R_{NaC2} + 0.40135∠NaC2C1 + 0.90620 ∠ONaC2; **e**(**6**) = 0.47461∠NaC2C1 − 0.87399∠H3OC2C1; **e**(**7**) = 0.72613∠NaOC2C1 + 0.6786∠H3OC2C1; **e**(**8**) = −0.99371∠NaOC2C1 − 0.11199∠H3OC2C1. (2) All the geometrical parameters of the transition states are intermediate to those of the two connected structures. Only the transition state **5** shows a large difference, but an intrinsic reaction coordinate (IRC) analysis with a large number of steps (n = 80) results in the following two structures (cf. figure below), both of which have larger ∠NaC2C1 than the transition state **5**. They are similar to structures **1** and **2**, respectively.

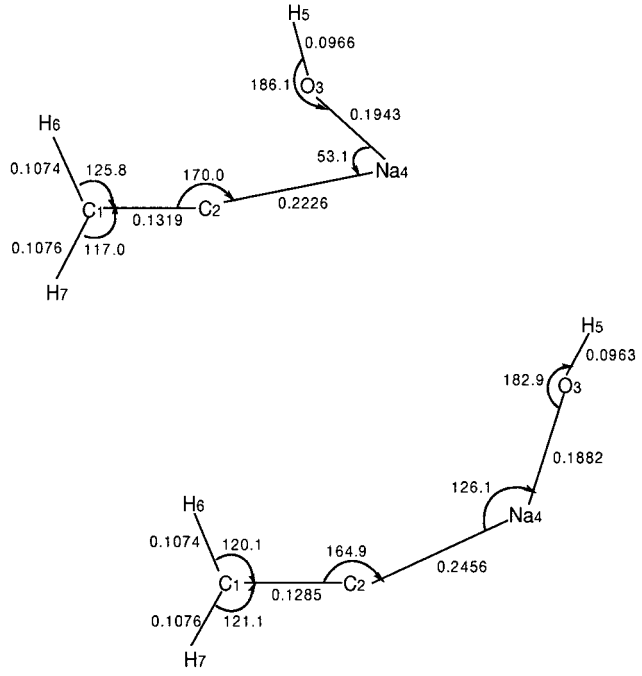

NPA analysis indicates that only structure **2** has net positive charge (+0.164) at the central carbon C2. FMO analysis shows that only structure **2**'s LUMO resembles the methylidene-carbene's (CH_2=C:) LUMO. The C_2 carbons in **1**, **3**, and **4** have net negative charges (−0.166 to −0.172 and −0.046, respectively). However, FMO analysis shows that only structure **4** puts more electron density on C_2 in the HOMO. Only structure **4** has a bare central carbon, which is ideal for carbanion-type reactions. In all, structure **1** is the most stable existing form for CH_2=CNa(OH). Structure **2** is important in carbenoid-type reactions, while structure **4** may play an important role in carbanion-type reactions.

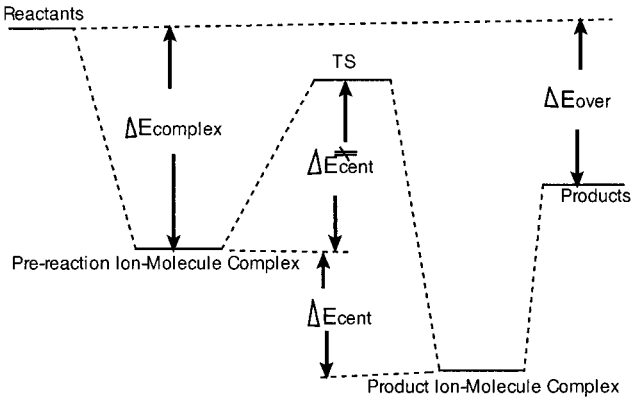

Figure 2. Schematic energy profile for the studied reactions.

Compared with the results calculated at the MP2/6-31+G* level of theory, the RHF/6-31+G* bond lengths of all structures and transition states are slightly shorter, whereas the bond angles are a bit larger. For example, at the MP2/6-31+G* level of theory, the C1−C2 bond lengths in **1** through **8** are 0.1346, 0.1299, 0.1359, 0.1362, 0.1300, 0.1349, 0.1350, and 0.1357 nm, respectively. The C1C2O bond angles for **1**, **3**, **4**, **6**, **7**, and **8** are 114.9°, 112.9°, 107.6°, 113.3°, 108.8°, and 112.1°, respectively. The RHF/6-31+G* approach significantly (by 40−50kJ/mol) overestimates the stability of the structures **2** and **5**, provided the results at the MP2/6-31+G* level of theory are correct, but the MP2(fu)/6-31+G* single point energies reproduce the trend within 10 kJ/mol. In all, the MP2(fu)/6-31+G*//RHF/6-31+G* approach describes reliably both structures and energies of the C_2H_3ONa isomerization process. Because the reactions studied here involve a large number of electrons and many possible intermediates and products, we also use the MP2-(fu)/6-31+G*//RHF/6-31+G* level of theory for the investigation in the following.

For all the reactions considered in the remainder of this work, we assume that their energy surface profiles can be represented by double-well potentials, as schematically shown in Figure 2. The reactions involve the initial formation of a prereaction ion−molecule complex, with a complexation energy $\Delta E_{complex}$, relative to the separated reactants, which then must overcome an activation barrier $\Delta E^{\ddagger}_{cent}$ to reach the transition structure (TS). The energy then drops as the product ion−molecule complex is produced, and the product ion−molecule complex may finally dissociate into the separated products. The overall energy change in the reaction is denoted as ΔE_{over}. The existence of pre- and postreaction ion−molecule complexes have been recently established experimentally[19] for some systems.

II. Reaction CH_2=CNa(OH) + CH_3^+ → CH_2=C(OH)CH_3 + Na^+

The carbanion-type reaction can be explained with two possible pathways.

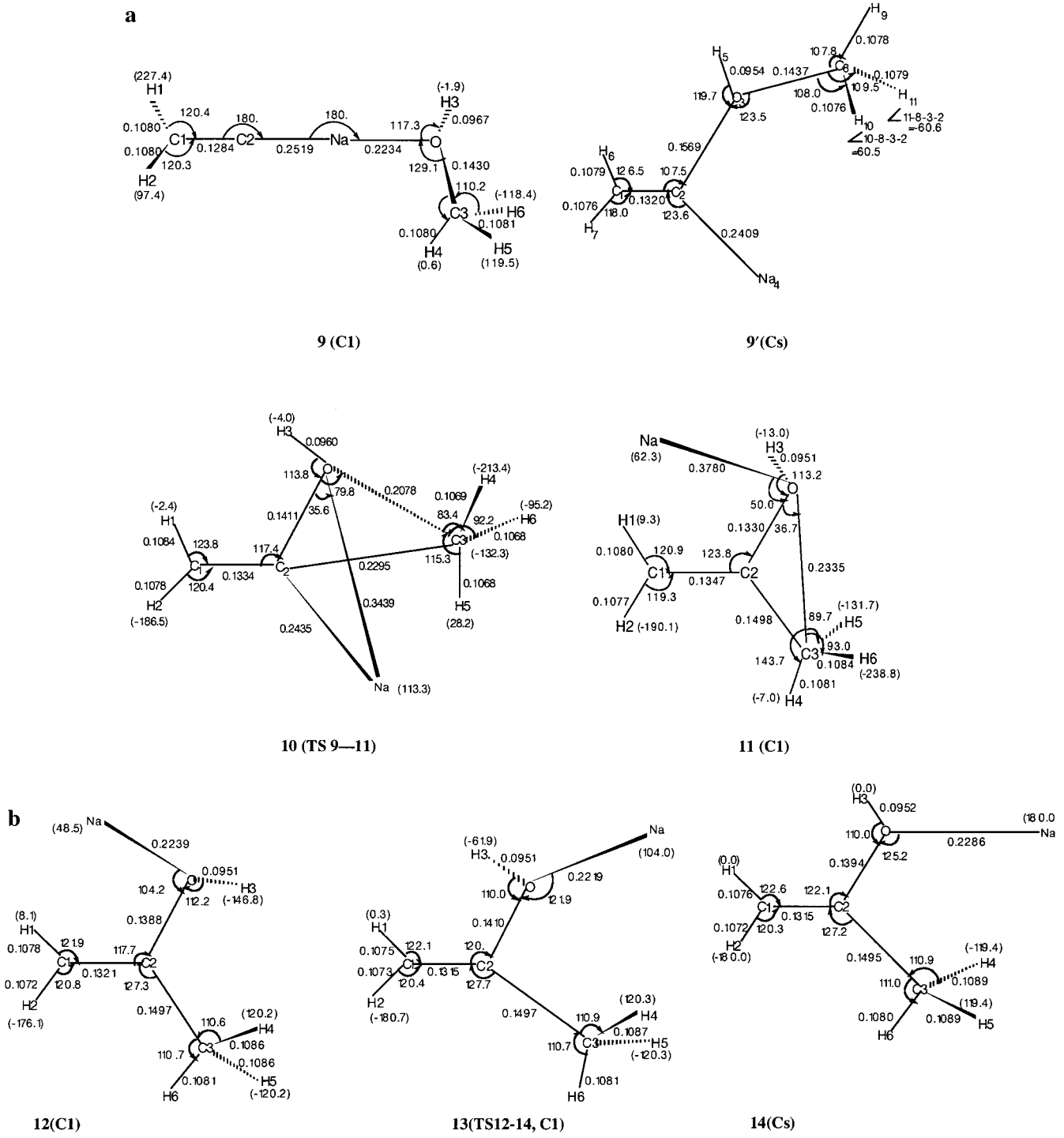

Figure 3. Structures and geometrical parameters for intermediates in reaction CH_2═C(OH)Na + CH_3^+ → CH_2═C(OH)CH_3 + Na^+ (RHF/6-31+G*, bond lengths in nm, bond angles in deg): (a) ion−molecule complexes and transition state for path A; (b) ion-molecule complexes and transition state for path B.

$$\mathbf{1} \xrightarrow{+CH_3^{\oplus}} \underset{\mathbf{9}\quad\mathbf{10}\quad\mathbf{11}}{\text{complex} \rightarrow \text{TS} \rightarrow \text{Complex}} \xrightarrow{-Na^{\oplus}} CH_2\text{=}C(OH)CH_3 \qquad \mathbf{A}$$

$$\mathbf{1} \xrightarrow{7} \mathbf{4} \xrightarrow{+CH_3^{\oplus}} \underset{\mathbf{12}\quad\mathbf{13}\quad\mathbf{14}}{\text{Complex} \rightarrow \text{TS} \rightarrow \text{Complex}} \xrightarrow{-Na^{\oplus}} CH_2\text{=}C(OH)CH_3 \qquad \mathbf{B}$$

In path **A**, the prereaction ion−molecule complex **9** is produced by the attachment of CH_3^+ to the oxygen of structure **1**. Then the CH_3^+ group moves from O toward the central carbon C_2 to give the product ion−molecule complex **11** via a transition state **10**. In path B, structure **1** isomerizes via transition state **7** into structure **4** before producing the ion−molecule complex **12** with CH_3^+. The ion−molecule complex **12** then changes into the ion−molecule complex **14** through transition state **13**.

The structures of ion−molecule complexes and transition states for path **A** are depicted in Figure 3a. Those for path B are given in Figure 3b. Their RHF/6-31+G* total energies, ZPEs, MP2(fu)/6-31+G* single point energies, and the relative energies are given in Table 2.

1. Geometries of Reactants and Products. Like other theoretical[20] and experimental[21] studies, our calculations show that CH_3^+ has a planar structure(D_{3h}). The product 2-hydroxyl-

TABLE 2: Total Energies, *E* (au), ZPEs[a] (kJ/mol), and Relative Energies, Δ(*E* + 2PE) (kJ/mol), for the Intermediates in the Reaction CH_2=C(OH)Na + CH_3+ → CH_2=C(OH)CH_3 + Na^+

	RHF/6-31+G*			MP2(fu)/6-31+G*//RHF/6-31+G*	
intermediates	*E*	ZPE	Δ(*E* + ZPE)	*E*	Δ(*E* + ZPE)
1 + CH_3^+	−353.356 07	212.2	711.6	−353.924 49	772.8
5 + CH_3^+	−353.307 08	193.8	823.7	−353.856 99	933.5
2 + CH_3^+	−353.308 32	193.2	819.8	−353.859 62	926.1
9	−353.514 95	233.7	308.1	−354.100 26	319.6
9′	−353.549 03	222.6	214.3	−354.114 17	284.1
10(TS9-11)	−353.435 27	227.6	517.4	−354.028 90	512.4
11	−353.635 11	241.3	5.0	−354.226 50	5.9
2-hydroxylpropene + Na^+	−353.598 63	238.6	98.3	−354.184 25	114.4
7 + CH_3^+	−353.341 93	211.8	748.5	−353.909 59	811.6
4 + CH_3^+	−353.344 14	212.7	743.4	−353.909 77	811.9
12	−353.636 76	240.6	0.0	−354.228 49	0.0
13(TS12-14)	−353.632 91	239.4	9.1	−354.223 10	13.1
14	−353.625 31	241.0	30.0	−354.214 71	36.0

[a] ZPEs are calculated at the RHF/6-31+G* level of theory and scaled by a factor 0.8929.

TABLE 3: Selected Parameters for Points at the *n*th Step along the Reaction Path in IRC Calculations (Bond Lengths in nm, Bond Angles in Degree)

n	R_{C2C1}	R_{C2O}	R_{C3O}	∠NaOC2C1	∠C3OC2C1
9′	0.1320	0.1569	0.1437	180	−180
9 (reactant)	0.1284	0.4753	0.1430	180	0[a]
110	0.1318	0.1655	0.1442	168.2	−107.1
80	0.1320	0.1597	0.1447	163.8	−116.5
60	0.1321	0.1557	0.1453	157.1	−117.4
30	0.1322	0.1492	0.1628	137.5	−119.7
10	0.1327	0.1440	0.1944	122.5	−126.5
TS**10** (transition state)	0.1334	0.1411	0.2078	113.3	−132.3
10	0.1347	0.1378	0.2172	103.7	−139.4
30	0.1367	0.1345	0.2253	86.9	−154.6
60	0.1362	0.1341	0.2341	69.6	−174.3
80	0.1344	0.1337	0.2317	65.0	−180.9
110	0.1345	0.1333	0.2338	64.0	−180.5
11 (product)	0.1347	0.1330	0.2335	62.3	−180.2

[a] 9 has a linear structure.

propene has C_s symmetry (see Figure 5). The reactant CH_2= C(OH)Na takes the form of structure **1**, for it is the lowest in energy among the four possible structures (cf. Figure 1).

2. Path A (See Figure 3a). The optimized prereaction ion−molecule complex **9** has a linear structure, with a completely broken C2−O bond. The expected structure denoted as **9′** is obtained as a local minimum only under the constraint of C_s symmetry. Structure **9′** has a lengthened C2−O bond (0.1569 nm) and a shortened C3−O bond (0.1437 nm, in methanol is 0.1425 nm[22]). Structure **9′** is 36.5kJ/mol higher in energy than structure **9** at the MP2(fu)/6-31+G*//HF/6-31+G* level of theory, and a frequency analysis indicates that **9′** has one imaginary frequency. In all, structure **9′** is not a local minimum, while structure **9** is the real prereaction ion−molecule complex. Because structure **9** is actually the complex of structure **2** and CH_3^+, the proposed path **A** should be revised to the following:

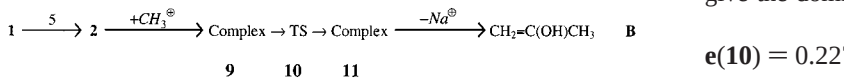

An additional step from structure **1** to **2** is needed.

In transition state **10**, C3 is nearly equidistant from the oxygen and the central carbon C2. These distances are long, while the C2−O bond is short. If we consider CH_3OH as a group, CH_3-OH moves toward C2 together at a nearly vertical direction with the C2−O bond more established. In the meantime, the C3−O bond in CH_3OH is breaking. Thus, the transition state **10** is a carbenoid type transition state for methylidenecarbene to insert into the C3−O bond of CH_3OH. NPA analysis indicates that the net charges on C3,O and C2 in **9** are −0.242, −0.903, and +0.087, while those in the transition state **10** are −0.021, −0.810, and −0.170, respectively. There is an electron flow from C3 to O then to C2, which indicates that this carbenoid mechanism is initiated by the attack of the electron-rich O to the empty p-orbital in the methylidenecarbene.

The optimized product ion−molecule complex **11** has a relatively long C1−C2 bond and has a Na^+ out of the C1C2O plane by 62.3°. The C1−Na, C2−Na, and O−Na distances are 0.2596, 0.3097, and 0.3780 nm, respectively. These facts mean that Na^+ interacts with the π-orbital of the C1−C2 double bond in product 2-hydroxylpropene.

To confirm our conclusions, we give the results of the transition vector, and we also use the reaction coordinate (IRC) method to follow the reaction path. The transition vector for TS **10** is as follows (there are 27 terms in all, and here we only give the dominate ones):

$$\mathbf{e}(\mathbf{10}) = 0.22787R_{C2O} - 0.32941R_{C3O} - 0.17025\angle OC2C1 + 0.76061\angle C3OC2 + 0.17597\angle C3OC2C1 + 0.22472\angle H4C3O - 0.34272\angle H5C3O$$

It is clear that the methyl group undergoes large movement, accompanied by the changes of C2−O and C3−O bond lengths. The selected parameters in IRC calculations are given in Table 3. From Table 3, we can see that the IRC calculations, starting from transition state **10**, can get closer to both reactant **9** and product **11** step by step. We can also see that the C2−O bond

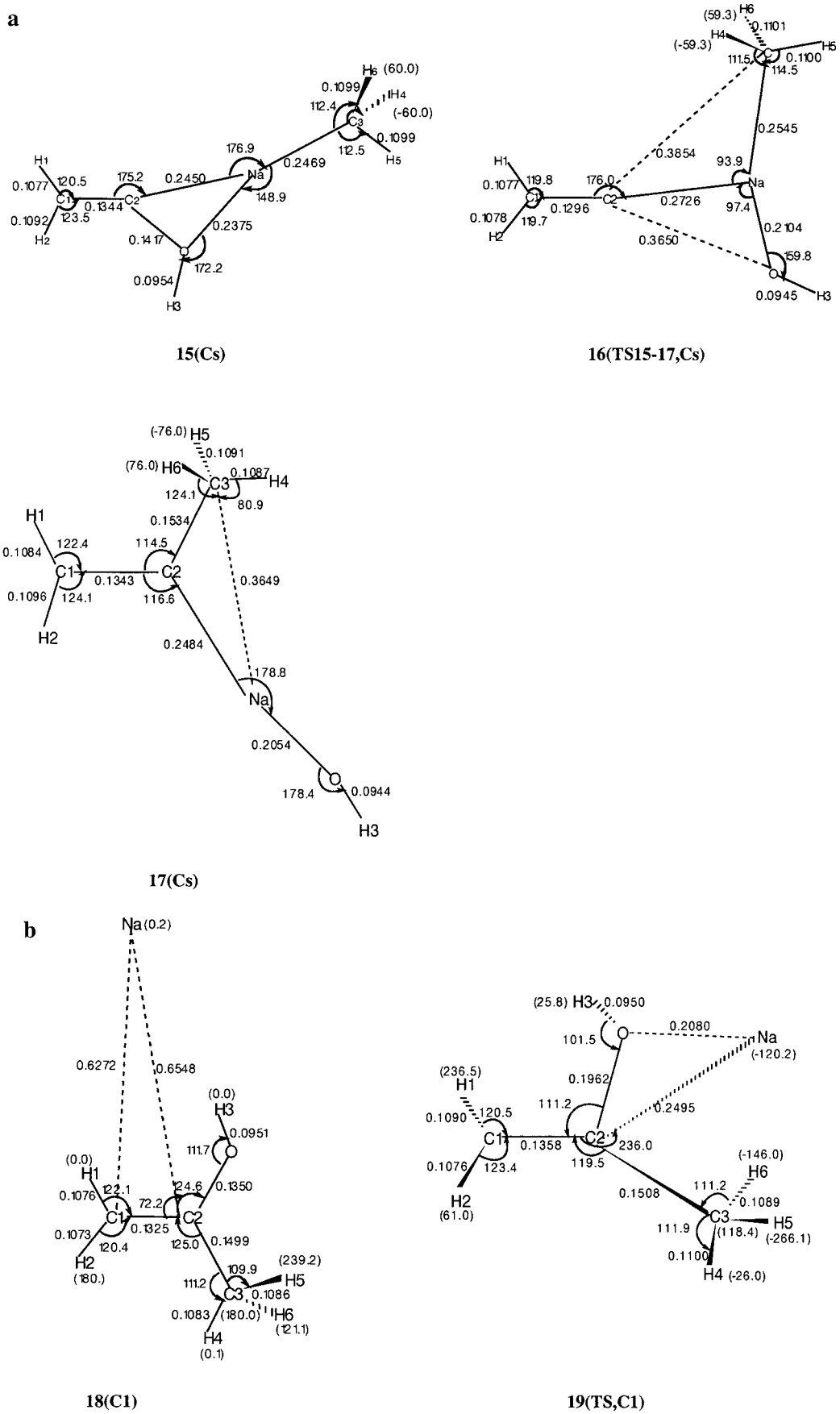

Figure 4. Structures and geometrical parameters for intermediates in reaction CH_2═C(OH)Na + CH_3^- → CH_2═C(CH_3)Na + OH^- (RHF/6-31+G*, bond lengths in nm, bond angles in deg): (a) ion−molecule complexes and transition state for path C; (b) ion−molecule complexes and transition state for path D.

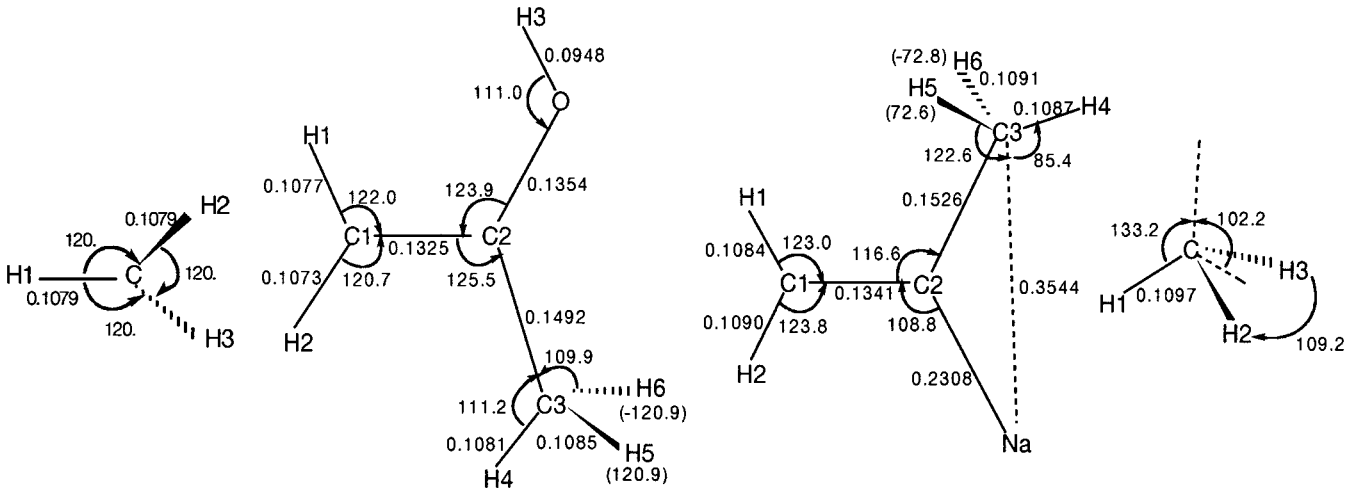

Figure 5. Geometries for separated reactants and products for the titled reactions (RHF/6-31+G*, bond lengths in nm, bond angles in deg). For CH_2=CNa(OH), see Figure 1.

TABLE 4: Total Energies (au), ZPEs[a] (kJ/mol), and Relative Energies, $\Delta(E + 2PE)$ (kJ/mol), for Intermediates of Reaction CH_2=C(OH)Na + CH_3^- → CH_2=C(CH_3)Na + OH^-

	RHF/6-31+G*			MP2(fu)/6-31+G*//RHF/6-31+G*	
intermediate	*E*	ZPE	$\Delta(E + ZPE)$	*E*	$\Delta(E + ZPE)$
1 + CH_3-	−353.629 33	203.2	348.6	−354.253 44	369.1
15	−353.717 95	209.5	121.6	−354.341 73	142.9
16	−353.643 15	188.4	299.2	−354.251 29	361.9
17	−353.766 34	215.6	0.0	−354.398 25	0.0
2-sodiumpropene + OH^-	−353.661 61	210.8	270.6	−354.295 91	264.4
18	−353.779 58	239.4	−13.6	−354.383 11	60.9
19	−353.650 81	220.0	307.2	−354.330 64	181.4

[a] ZPEs are calculated at the RHF/6-31+G* level of theory and scaled by 0.8929.

is lengthened steadily and is longer than the C2−O bond length of **9′** after $n = 80$ steps.

3. Path B (See Figure 3b). Complex **12** is the ion−molecule complex of CH_3^+ and structure **4** as expected. It is certain that structure **14** is the ion−molecule complex of product 2-hydroxylpropene and Na^+.

Complex **12**, transition state **13**, and complex **14** are very close in energy. Both complex **12** and complex **14** have geometrical parameters similar to those of product 2-hydroxylpropene. Complex **12** has Na^+ and H3 out of the C1C2O plane, while complex **14** has them in the C1C2O plane. In fact, structure **13** is the transition state of the C2−O rotation, and the activation barrier is small (13.1 kJ/mol at the MP2(full)/6-31+G*//RHF/6-31+G* level of theory). The configuration of C2 is retained in this transition state.

4. Reaction Mechanism. Both paths **A** and **B** involve two elementary steps. The two activation barriers ($\Delta E^{\ddagger}_{cent}$) for path **A** are 112.1 and 181.9 kJ/mol, whereas those for path **B** are 38.8 and 13.1 kJ/mol; i.e., path **B** is favorable. The reaction is largely exothermic (the overall reaction energy ΔE_{over} is 658.4 kJ/mol).

5. Comments on product ion−molecule complexes 11 and 14. There are two favorable factors in product 2-hydroxylpropene for Na^+ to form the product ion−molecule complexes. One is the lone pair on oxygen, and the other is the π-bond. These lead to different ion−molecule complexes **11** and **14**, with which **11** is 30 kJ/mol higher in energy at the RHF/6-31+G* level of theory. If we check transition state **10** in detail, we find that the C1−C2 distance in TS **10** is also longer than C1−C2 distances in both reactant **9** and product 2-hydroxylpropene; then we conclude that in TS **10**, CH_3^+ plays a role in interaction with the π-bond in carbene when O interacts with the empty p-orbital.

III. Reaction CH_2=CNa(OH) + CH_3^- → CH_2=CNa(CH_3) + $^-$OH

An α-alkali metal unsaturated ether can react with nucleophiles such as R′Li, whereby the heteroatom is substituted by R′, accompanied by the inversion of the configuration of central carbon.[7,23,24] It is the typical reaction only of carbenoids. There are two proposals for the reaction mechanism. The first proposal believes that the attachment of R'^- forms a metalate, in which an intramolecular 1,2-migration of R′ and a substitution of the alcoholate takes place. The inversion of the configuration of the carbenoid carbon atom has been established without doubt.[25] The second proposal believes that the breaking of the C−OR bond leads to a contact ion pair. The backside attack of R'^- will replace OR^- with the inversion of the configuration of the carbenoid carbon atom.[26,27]

Since both proposals may demand the same transition state, we propose the following mechanism:

$$\mathbf{1} \xrightarrow{+CH_3^-} \underset{\mathbf{15}}{\text{Complex}} \rightarrow \underset{\mathbf{16}}{\text{TS}} \rightarrow \underset{\mathbf{17}}{\text{Complex}} \xrightarrow{-OH^-} CH_2{=}C(CH_3)Na \qquad \mathbf{C}$$

Nucleophilic vinylic substitution often proceeds via an addition−elimination pathway, initiated by a nucleophilic attack at the π-bond. This may involve a multistep pathway via one or more carbanion intermediates or a single-step process when

TABLE 5: Relative Energies (kJ/mol) of Transition States 16 and 19 in Different Solvents

TSs	gas phase ($\epsilon = 0.0$)	cyclohexane ($\epsilon = 2.0$)	1,2-dichloroethane ($\epsilon = 10.1$)	acetonitrile ($\epsilon = 35.9$)
16	0	0	0	0
19	−20.0	−3.5	19.2	23.9

TABLE 6: Relative Energies (kJ/mol)[a] of Transition States 16 and 19 at Different Calculation Levels

TSs	RHF/6-31+G*	MP2(full)/6-31+G*//RHF/6-31+G*	MP2/6-31+G*//MP2/6-31+G*	B3LYP/6-31+G*//B3LYP/6-31+G*
16	0	0	0	0
19	8.0	−180.1	−177.5	−109.9

[a] With ZPE correction.

substitution reduces the lifetime of the carbanion intermediate(s) to zero. Both the stepwise and the concerted processes normally lead to the retention of the configuration.[28−30] We also briefly investigate the following pathway **D** on the consideration of the similarity of the two reactions.

$$\mathbf{1} \xrightarrow{+CH_3^-} \underset{\mathbf{18}}{\text{carbanion}} \rightarrow \underset{\mathbf{19}}{\text{TS}} \rightarrow \underset{\mathbf{17}}{\text{Complex}} \xrightarrow{-OH^-} CH_2{=}C(CH_3)Na \qquad \mathbf{D}$$

The structures and geometrical parameters of the ion−molecule intermediates and the transition state for path **C** are depicted in Figure 4a. Those for path **D** are given in Figure 4b. Their total RHF/6-31+G* energies, ZPEs, single point energies calculated at the MP2(fu)/6-31+G* level of theory, and relative energies are given in Table 4.

1. Geometries of Reactants and Products. Like other authors' results,[31] our calculations show that CH_3^- has pyramidal structure (C_{3v}), and product 2-sodiopropene has C_s symmetry (see Figure 5).

2. Path C (See Figure 4a). In prereaction ion−molecule complex **15**, the attachment of CH_3^- does not change **1** significantly, which means that the complexation of CH_3^- to Na can compensate the unfavorable "Umpolung" in structure **1** to some degree.

The geometry of transition state **16** clearly shows the inversion of the configuration of the carbenoid carbon atom. In the TS **16**, the C2−O distance is very long (0.3854 nm, already broken), and the C2−C3 distance is very long (0.3650 nm, bond not yet established). That is an indication of the "metal-assisted ionization" mechanism. Moreover, the geometrical parameters of **16** are very similar to those of structure **2**, and the NPA analysis shows that the OH group in both **16** and **2** holds a large amount of negative charge (−0.97 and −0.96, respectively).

To say **17** is the product ion−molecule complex is reasonable.

3. Path D (See Figure 4b). When we try to optimize the anion intermediate without any constraints, we get complex **18**, as shown in Figure 4b). Complex **18** does not have a sp^3-hybridized C2, which should exist in an anion intermediate, but has a sp^2-hybridized one with the Na distant from C1 and C2. The NPA analysis shows that Na holds a large amount of negative charge (−0.996). The unfavorable "Umpolung" of C2 is now shifted to Na, which may be even more unfavorable, because the alkali metals have only a rather small electron affinity. Thus, we do not think that **18** is a prereaction ion−molecule complex.

We initially want transition state **19**, which has some character of π-bond attack. When we check it carefully, we find C1, C2, Na, C3 and H1, H2 are almost in one plane, and both the C3−C2 distance and C2−O distance are short, which may contribute to the inversion of the configuration of the central carbon but lose π-bond attack character. IRC analysis with a large number of steps ($n = 80$) gives the following two structures,

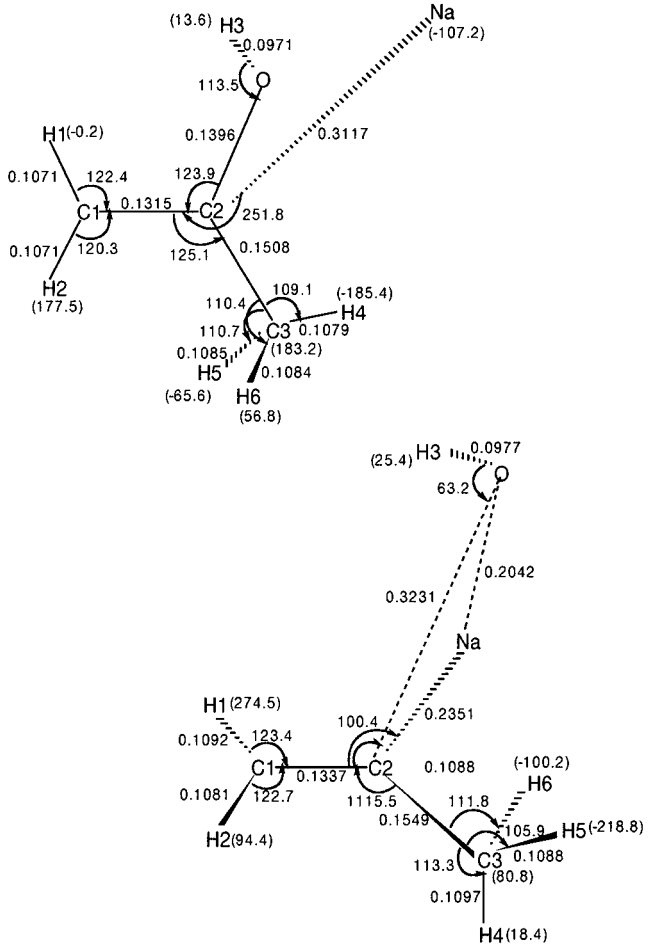

which are similiar to **18** and **17**, respectively. In all, path **D** is not what we wanted.

4. Reaction Mechanism. The reaction proceeds through path **C**, and the "metal-assisted ionization" mechanism is reasonable. The overall reaction energy ΔE_{over} is 104.7 kJ/mol.

5. Comments on Path D. Although path **D** is not what we wanted, it interested us to check solvent effects and the reliability of our calculations. The relative energies for TS **16** and TS **19** in different slovents at the RHF/6-31+G* level of theory are given in Table 5. The relative energies obtained at different calculation levels are given in Table 6. B3LYP is the density function theory method introduced by Becke[32,33] and is available in Gaussian 98.

From Table 5, we can see that highly polar solvents (with high dielectric constants (ϵ)) favor transition state **16**. From Table 6, we can see that MP2(fu)/6-31+G*//RHF/6-31+G* is still comparable to MP2/6-31+G*//MP2/6-31+G*. Density function theory has been tested to have a higher accuracy than that corresponding to the MP2 level of theory;[34] then we know

that both the above MP2 calculation levels overestimate the differences between TS **16** and TS **19**.

Conclusions

The conclusions of this work may be summarized as follows:

(1) When CH_2═CNa(OH) reacts with CH_3^+, it first isomerizes from three-member-ring **1** to nonplanar structure **4**, then reacts with the electrophiles. The carbenoid type mechanism is unlikely to happen.

(2) When CH_2═CNa(OH) reacts with CH_3^-, it breaks the C−O bond to produce a contact ion pair, followed by the attack of the nucleophile from the backside. The backside attack leads to the inversion of the configuration of the central carbon.

(3) The MP2(fu)/6-31+G*//RHF/6-31+G* level of calculation is comparable to the MP2/6-31+G*//MP2/6-31+G* one both in the isomerization process of C_2H_3ONa and in the title reactions.

References and Notes

(1) Verkruijsse, H. D.; Brandsma, L.; Schleyer, P. V. R. *J. Organomet. Chem.* **1987**, *332*, 99.
(2) Seebach, D. *Angew Chem., Int. Ed. Engl.* **1969**, *8*, 639.
(3) Söllkopf, U.; Hänssle, P. *Justus Liebigs Ann. Chem.* **1972**, *763*, 208.
(4) Baldwin J. E.; Höfle G. A.; Lever O. W., Jr. *J. Am. Chem. Soc.* **1974**, *96* (22), 7125.
(5) Stang, P. J. *Acc. Chem. Res.* **1978**, *11*, 107.
(6) Schöllkopf, U. *Angew. Chem., Int. Ed. Engl.* **1970**, *9* (10), 763.
(7) Boche, G.; Lohrenz, J. C. W.; Opel, A. *Lithium Chemistry: A Theoretical and Experimental Overview*; Spase, A.-M., Schleyer P. V. R., Eds.; John Wiley and Sons: New York, 1995; pp 209−215.
(8) Wang, Y.; Sun, C.; Deng, C. *J. Phys. Chem. A* **1998**, *102* (29), 5816.
(9) Schaefer, H. F., III; Yamaguchi, Y. *J. Mol. Strut. (THEOCHEM)* **1986**, *135*, 369.
(10) Clark, T.; Chandrasekhari, J.; Spitznagel, G. W.; Schleyer, P. V. R. *J. Comput. Chem.* **1983**, *4*, 294.
(11) Curtiss L. A.; Raghavachari K.; Trucks G. W. *J. Chem. Phys.* **1991**, *94*, 7221.
(12) Reed A. E.; Carpenter J. E.; Weinhold F. *NBO Version 3.1*; Gaussian, Inc.: Pittsburgh, PA, 1992.
(13) Fukui, K. *Acc. Chem. Res.* **1981**, *14*, 363.
(14) Gonzalez, C.; Schlegel, H. B. *J. Phys. Chem.* **1990**, *94*, 5523.
(15) Tapia, O.; Goscinski, O. *Mol. Phys.* **1975**, *29*, 1653.
(16) Wiberg, K. B.; Murcko, M. A. *J. Phys. Chem* **1987**, *91*, 3616.
(17) Frisch, M. J.; Trucks, G. W.; Head-Gordon, M.; Gill, P. M. W.; Wong, M. W.; Foresman, J. B.; Johnson, B. G.; Schlegel, H. B.; Robb, M. A.; Replogle, E. S.; Gomperts, R. Andres, J. L.; Raghavachari, K.; Binkley, J. S.; Gonzalez, C.; Martin, R. L.; Fox, D. J.; Defrees, D. J.; Baker, J.; Stewart, J. J. P.; Pople, J. A. *Gaussian 92*, Revision F.4; Gaussian, Inc.: Pittsburgh, PA, 1992.
(18) Frisch, M. J.; Trucks, G. W.; Schlegel, H. B.; Scuseria, G. E.; Robb, M. A.; Cheeseman, J. R.; Zakrzewski, V. G.; Montgomery, J. A.; Stratmann, R. E.; Burant, J. C.; Dapprich, S.; Millam, J. M.; Daniels, A. D.; Kudin, K. N.; Strain, M. C.; Farkas, O.; Tomasi, J.; Barone, V.; Cossi, M.; Cammi, R.; Mennucci, B.; Pomrlli, C.; Adamo, C.; Clifford, S.; Ochterski, J.; Petersson, G. A.; Ayala, P. Y.; Cui, Q.; Morokuma, K.; Malick, D. K.; Rabuck, A. D.; Raghavachari, K.; Foresman, J. B.; Cioslowski, J.; Ortiz, J. V.; Stefanov, B. B.; Liu, G.; Liashenko, A.; Piskorz, P.; Komaromi, I.; Gomperts, R.; Martin, R. L.; Fox, D. J.; Keith, T.; Al-Laham, M. A.; Peng, C. Y.; Nanayakkara, A.; Gonzalez, C.; Challacombe, M.; Gill, P. M. W.; Johnson, B. G.; Chen, W.; Wong, M. W.; Andres, J. L.; Head-Gordon, M.; Replogle, E. S.; Pople, J. A. *Gaussian 98*, Revision A.1; Gaussian, Inc.: Pittsburgh, PA, 1998.
(19) Cyr. D. M.; Bishea, G. A.; Scarton, M. G.; Johnson, M. A. *J. Chem. Phys.* **1992**, *97*, 5911.
(20) Raghavachari, K.; Whiteside, R. A.; Pople, J. A.; Schleyer, P. V. R. *J. Am. Chem. Soc.* **1981**, *103*, 5649.
(21) Fort, R. C. In *Carbonium Ions*, Olah, G. A., Schleyer, P. V. R., Eds.; John Wiley and Sons: New York, 1973; Vol. IV; p 1783.
(22) Sette, F.; Stör, J.; Hitchcock, A. P. *J. Chem. Phys.* **1984**, *81*, 4906.
(23) Kocienski P.; Barber C. *Pure Appl. Chem.* **1990**, *62*, 1933.
(24) Nguyen, T.; Negishi, E. *Tetrahedron Lett*. **1991**, *32*, 5903.
(25) Kocienski, P.; Wadman, S. *J. Am. Chem. Soc.* **1989**, *111*, 2363.
(26) Köbrich G. *Angew. Chem., Int. Ed. Engl.* **1972**, *11*, 1 (6), 473.
(27) Duraisamy M.; Walborsky H. M. *J. Am. Chem. Soc.* **1984**, *106*, 5035.
(28) Rappoport, Z. *Acc. Chem. Res.* **1981**, *14*, 7.
(29) Rappoport, Z. *Acc. Chem. Res.* **1992**, *25*, 474.
(30) Glukhovtsev, M. N.; Pross, A.; Radom, L. *J. Am. Chem. Soc.* **1994**, *116*, 5961.
(31) Jemmis, E. D.; Buss, V.; Schleyer, P. V. R.; Allen, L. C. *J. Am. Chem. Soc.* **1976**, *98*, 6483.
(32) Becke, A. D. *J. Chem. Phys.* **1993**, *98*, 5648.
(33) Becke, A. D. *Phys. Rew. A* **1988**, *38*, 3098.
(34) Foresman, J. B.; Frisch A. *Exploring Chemistry with Electronic Structure Methods: A Guide to Using Gaussian, 2nd ed.;*, Gaussian, Inc.: Pittsburgh, PA, 1996; p 141.